ELSEVIER

Sensors and Actuators A 55 (1996) 35–41

SENSORS AND ACTUATORS A PHYSICAL

Electrothermal responses of lineshape microstructures

Liwei Lin, Mu Chiao

Institute of Applied Mechanics, National Taiwan University, Taipei, Taiwan

Abstract

Electrothermal responses of attached and suspended lineshape microstructures fabricated by surface micromachining are investigated. A three-dimensional electrothermal model has been established. This model is based on an axial, one-dimensional electrothermal analysis and a heat-conduction shape factor that represents heat transfer perpendicular to the axial direction. Experimental devices have been built by the surface-micromachining process and a 2 μm gap is constructed for suspended microstructures. Electrical power is passed through these microstructures to characterize the electrothermal responses. Bubble-formation experiments which use local electrical heating to generate micro thermal bubbles in a working liquid have been tested by using these microstructures and the experimental results are consistent with the theoretical model.

Keywords: Electrothermal response ; Lineshapes ; Surface micromachining

1. Introduction

Electrothermal responses are important for microsystems sensitive to thermal effects. For example, bubble jet printers use electrothermally generated microbubbles to eject ink for printing [1]. Thermally excited microactuators [2] and thermal flow meters [3,4] are applications among many others that use electrothermal reactions as the operation principle in microsystems. Three types of microstructures can be identified in the above applications: attached microstructures fabricated by a general IC process; overhanging microstructures fabricated by bulk micromachining; and suspended microstructures fabricated by surface micromachining. In order to understand fully the electrothermal characteristics of these microstructures, process-independent analysis is essential.

Previously, electrothermal models for lineshape microstructures attached to a silicon substrate have been studied [5]. Models for lineshape suspended microstructures have also been studied without considering the heat transfer in the plane perpendicular to the device axial direction [6] or without considering the effect of passivation layers [7]. This paper describes a process-independent electrothermal model by considering all heat-transfer effects. Moreover, both *I–V* measurements and bubble-generation experiments used as a temperature monitor [5] are used for verification of the analytical model.

PII S0924-4247(96)01247-2

2. Microstructure design and fabrication

Fig. 1 shows a schematic diagram of the suspended and attached microstructures tested in this paper. They are made of heavily phosphorus-doped polysilicon with different deposition recipes in a standard surface-micromachining process [8]. The gap between the substrate and suspended microstructure is 2 μm. The thicknesses of the silicon nitride and oxide layers are 0.4 and 0.5 μm, respectively, and both layers function as electrical and thermal insulation materials. A current I can be sent through contact pads to the microstructures for measuring electrothermal responses.

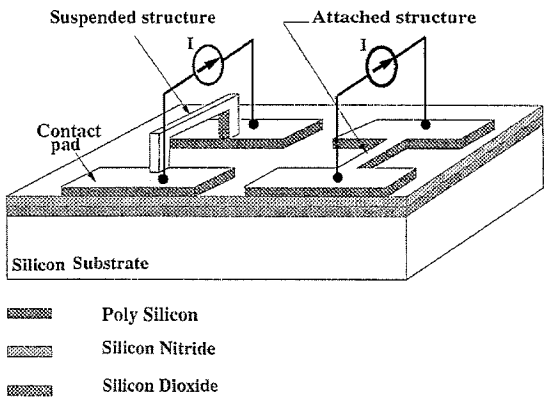

Fig. 1. Schematic diagram of suspended and attached microstructures.

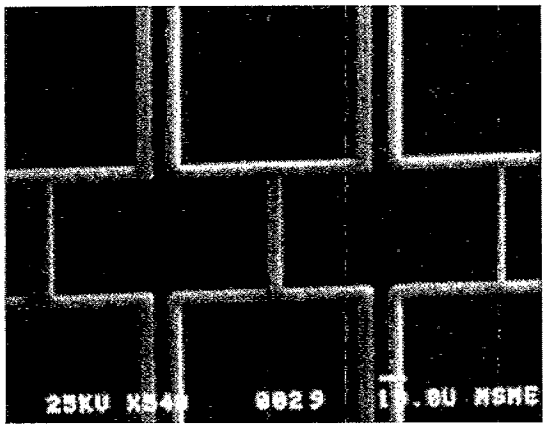

Fig. 2. SEM micrograph of three lineshape suspended microstructures with length of 50 μm and widths of 10, 5 and 2 μm.

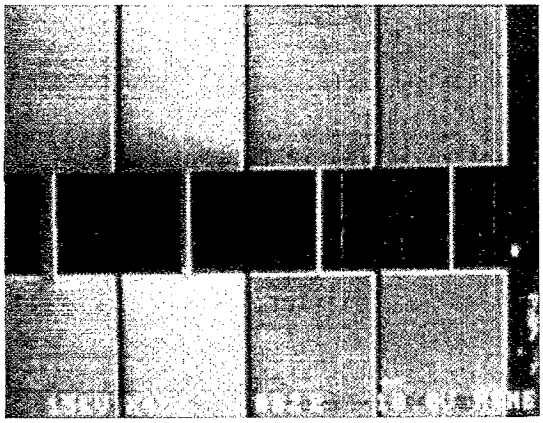

Fig. 3. Fabricated attached-type microstructures with length of 50 μm and widths of 10, 5, 2 and 1 μm.

Two sets of microstructures, of suspended and attached type, have been fabricated on the same chip. Each set has a group of microstructures with lengths of 10, 50 and 100 μm and widths of 1, 2, 5 and 10 μm. The attached-type microstructures use an LPCVD in situ phosphorus-doping process to grow a 0.5 μm thick layer of heavily phosphorus-doped polysilicon. The deposition pressure is 300 mTorr and the temperature is 610 °C with 120 sccm of SiH_4 and 1 sccm of PH_3 flowing. The suspended microstructures use a 1000 °C, two hour drive-in process for the phosphorus doping. After the sacrificial PSG (phosphorus-doped glass) layer deposition in a surface-micromachining process [8], a layer of undoped polysilicon is deposited. The deposition pressure is 550 mTorr at 605 °C with 250 sccm of SiH_4 flowing. A second PSG layer is deposited on top of the undoped polysilicon layer and phosphorus is doped from the top and bottom of the polysilicon layer during the drive-in process. Fig. 2 is an SEM micrograph of three suspended microstructures. They are 50 μm long, 10, 5 and 2 μm wide (from left to right), respectively. Light coloured areas in the micrograph are the suspended portions standing 2 μm above the substrate. Fig. 3 is an SEM micrograph of a set of attached-type microstructures. They are 50 μm long and 10, 5, 2 and 1 μm in width, respectively.

3. Theoretical analysis

3.1. Heat equation

A one-dimensional model including a correction number, the shape factor, for the other two missed dimensions is established for these lineshape microstructures. A second-order partial differential heat equation can be derived for both attached and suspended microstructures based on the law of conservation of energy [9]:

$$\frac{\partial^2 T}{\partial x^2}=\frac{1}{\alpha_p}\frac{\partial T}{\partial t}+\epsilon(T-T_r) \tag{1}$$

in which T is the temperature along the microstructure, t stands for time, α_p is the thermal diffusivity of polysilicon and ϵ, T_r are parameters that are functions of the structure dimension and thermal properties, as summarized below:

- Attached microstructure

$$\alpha_p=\frac{k_p}{c_p\rho_p} \tag{2}$$

$$\epsilon=\frac{k_{att}F_{s,att}}{k_p h(t_n+t_o)}-\frac{J^2\rho_0\xi_p}{k_p} \tag{3}$$

$$T_r=T_\infty+\frac{J^2\rho_0}{k_p\epsilon} \tag{4}$$

- Suspended microstructure

$$\alpha_p=\frac{k_p}{c_p\rho_p} \tag{5}$$

$$\epsilon=\frac{k_{sus}F_{s,sus}}{k_p h(t_n+t_o+lift)}-\frac{J^2\rho_0\xi_p}{k_p} \tag{6}$$

$$T_r=T_\infty+\frac{J^2\rho_0}{k_p\epsilon} \tag{7}$$

where k_{att} and k_{sus} are the combined thermal conductivity for attached and suspended microstructures, respectively, which can be expressed as

$$k_{att}=\frac{k_n k_o(t_n+t_o)}{k_o t_n+k_n t_o} \tag{8}$$

$$k_{sus}=\frac{k_n k_o k_{fd}(t_n+t_o+lift)}{k_{fd}k_o t_n+k_{fd}k_n t_o+k_n k_o lift} \tag{9}$$

The excessive heat-flux shape factors $F_{s,att}$ and $F_{s,sus}$ for the attached and suspended microstructures are defined as

$$F_{s,att}=\frac{\text{total heat conduction per unit length}}{[wk_{att}(T-T_\infty)]/(t_n+t_o)} \tag{10}$$

$$F_{s,sus}=\frac{\text{total heat conduction per unit length}}{[wk_{sus}(T-T_\infty)]/(t_n+t_o+lift)} \tag{11}$$

The shape factor is defined as the total heat flux out of the lineshape microstructure per unit length divided by the heat flux going directly under the width of the microstructure as

shown. The purpose of introducing this factor is to account for the excessive heat fluxes that are not included in the original model. In this way, the heat conducted to the environment is included in the excessive-flux shape factor for more accurate modelling. For attached microstructures, the heat conducted to the substrate dominates the heat-transfer process. For suspended microstructures, the gap between the microstructure and the substrate results in a better thermal isolation such that the excessive-heat-flux shape factor is expected to increase.

3.2. Steady state and transient solutions

3.2.1. Steady state solution

The steady state solution of the heat equation is solved subject to initial and boundary conditions by assuming that both ends of the lineshape microstructure remain at the ambient temperature during the heating process and the microstructure is initially at the ambient temperature before heating. That is:

$$T(x=0,\ t)=T_\infty \tag{12}$$

$$T(x=L,\ t)=T_\infty \tag{13}$$

$$T(x,\ t=0)=T_\infty \tag{14}$$

The steady state solution of the temperature distribution along a lineshape microstructure is

$$T(x)_{ss}=T_r-(T_r-T_\infty)\frac{\cosh\left[\sqrt{\epsilon}\left(x-\frac{L}{2}\right)\right]}{\cosh\left(\sqrt{\epsilon}\frac{L}{2}\right)} \tag{15}$$

The maximum temperature can be derived from the steady state solution by differentiating the above equation, which gives

$$T_{ss,max}=T_r-(T_r-T_\infty)\frac{1}{\cosh\left(\sqrt{\epsilon}\frac{L}{2}\right)} \tag{16}$$

It is noted in Eq. (16) that $T_{ss,max}$ depends on both ϵ and T_r. Since the electrical current density, J, is the only variable for both ϵ and T_r, a desirable $T_{ss,max}$ can be reached by adjusting J.

3.2.2. Transient solution

The transient solution of temperature distribution is

$$T(x,t)=\exp(-\alpha\epsilon t)\sum_{n=1}^{\infty}B_n\sin\left(\frac{n\pi x}{L}\right)\exp[-\alpha_p t(nx/L)^2] \tag{17}$$

where

$$B_n=\frac{2}{L}\int_0^L[T_\infty-T(x)_{ss}]\sin\left(\frac{nx}{L}\right)dx \tag{18}$$

By examining the transient solution, it is found that the slowest transient decay time ($n=1$) is of the order of 10 μs. For an input source of frequency less than 10 kHz, the microstructure temperature reaches the steady state temperature without significant transient delay.

3.3. Electrothermal characteristics

The electrical model including voltage and current can be found by deriving the resistance of a lineshape microstructure. The resistance depends on temperature changes and can be calculated as

$$R=\int_0^L dR(T)=\frac{\rho_0 L}{wh}[1+\xi_p(T_{avg}-t_\infty)] \tag{19}$$

where T_{avg} stands for the average temperature of the microstructure and can be expressed as

$$T_{avg}=\frac{1}{L}\int_0^L T dx=T_r-(T_r-T_\infty)\frac{\tanh\left(\sqrt{\epsilon}\frac{L}{2}\right)}{\sqrt{\epsilon}\frac{L}{2}} \tag{20}$$

These equations are useful for calculating the electrical power consumption.

4. Numerical simulations

4.1. Shape factor

The finite-element simulation software, ANSYS [10], is used to calculate steady state heat-transfer characteristics. Fig. 4 is the cross-sectional region which has been filled with about 2000 finite-element meshes around a half of the suspended microstructure. The simulated microstructure is 4 μm in total width, 2 μm in thickness and 2 μm in suspension distance. When the structure is immersed in water and heated to a high temperature, isotherms are simulated as plotted in Fig. 5. It is observed that most of the heat-transfer process

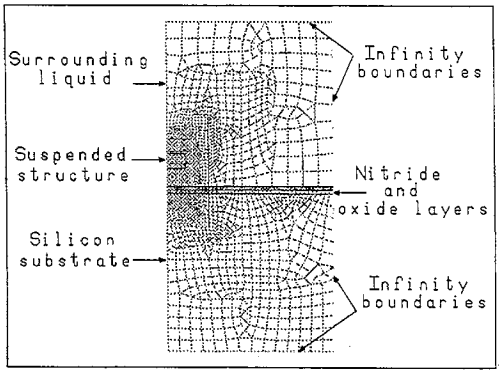

Fig. 4. Finite-element meshes for cross section of a lineshape suspended microstructure. Only half the structure is simulated.

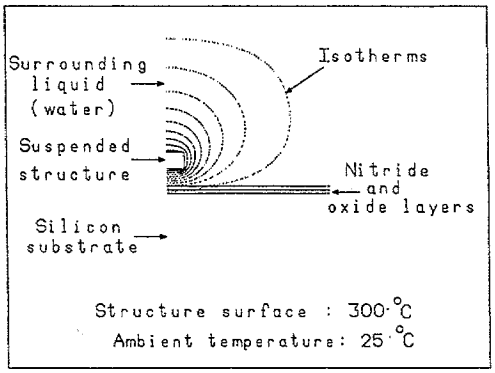

Fig. 5. Isotherms of a suspended microstructure which is 4 μm wide, 2 μm thick and suspended 2 μm above substrate.

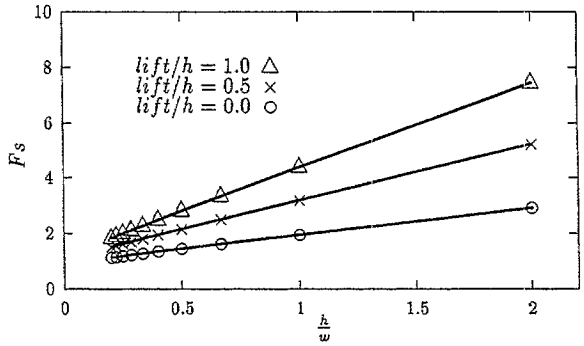

Fig. 6. Shape factor vs. h/w for different types of microstructures in water.

occurs in a very small region around the microstructure and major heat fluxes are flowing downward to the substrate.

Results from finite-element simulation are used to calculate the shape factors, F_s, which affect the overall heat-transfer process. Structures with different cross sections and suspension gaps in water have been simulated as shown in Fig. 6, where F_s is plotted with respect to a non-dimensional variable h/w (thickness of a microstructure over its width). Three cases, $lift/h=0$, $lift/h=0.5$ and $lift/h=1$, have been plotted with the thickness of microstructures fixed at 2 μm. As observed in Fig. 6, if the h/w value is fixed, the shape factor increases as the suspension distance increases. It is also noted that F_s increases linearly with respect to h/w and the slopes of these lines are found to be 1.00, 2.06 and 3.12, respectively. An empirical expression for the shape factors can be expressed as

$$F_s=\frac{h}{w}\times\left(2\times\frac{lift}{h}+1\right)+1 \qquad (21)$$

4.2. Power consumption

The power-consumption rate can be simulated to evaluate device performance. Eq. (16) is solved by the Newton method to obtain the current density, J. The resistance, R, is then calculated by using Eq. (19) and Eq. (20) to obtain the electrical power. Fig. 7 shows the simulation result of electrical power with respect to length of suspended and attached

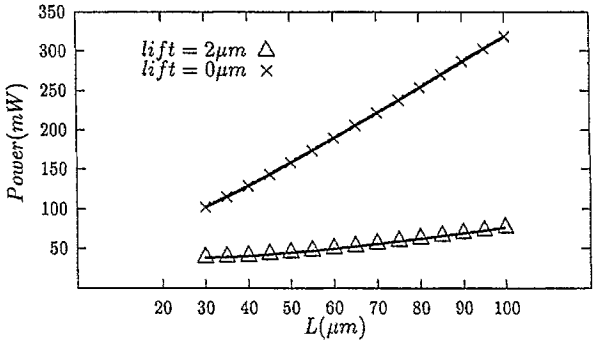

Fig. 7. Power consumption vs. structure length for lineshape microstructures with a cross section of 4 μm in width and 2 μm in thickness.

microstructures, respectively. Both types of microstructures used in simulation have a cross section of 4 μm in width and 2 μm in thickness and the suspension distance is 2 μm. It is observed in Fig. 7 that only about 50 mW of power is needed for suspended microstructures with a length up to 100 μm. However, the power consumption reaches 300 mW for attached microstructures when they are longer than 100 μm.

5. Experiments

Both suspended and attached microstructures were tested and compared with theoretical models. Experiments are carried out under a probe station, observed via a microscope and recorded on a video tape. One silicon die including both testing structures was cut out of a silicon wafer and fixed with tapes on the bottom of a shallow beaker. Flourinert 43 (an electronic cooling liquid provided by 3M Company) was then put into the beaker until the liquid depth reached 2 mm. All the experiments were carried out at room temperature and under one atmosphere pressure.

5.1. I–V characteristic curve

Basic electrothermal characteristics have been studied by comparing theoretical and experimental I–V curves in an air environment. Fig. 8 shows measurement results of I–V curves for two groups of attached microstructures. The measurements stop when the applied power is too high and the current reading is unstable. Solid lines in Fig. 8 are simulation results

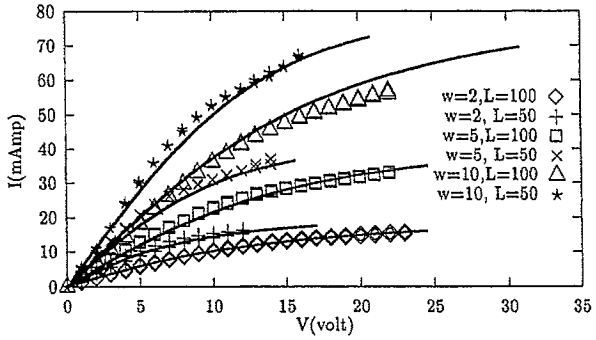

Fig. 8. I–V curves of attached microstructures.

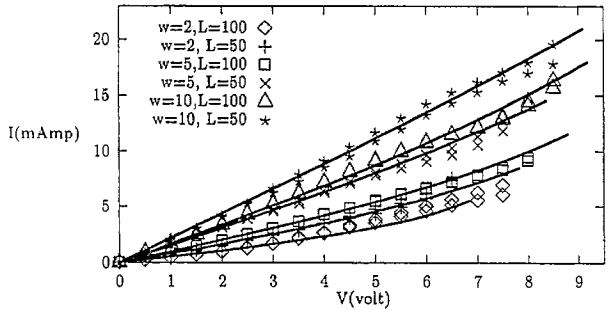

Fig. 9. *I–V* curves of suspended-type microstructures.

according to our analytical model. It is found by the best curve-fitting method that the temperature coefficient of the polysilicon resistivity is $2.00\times10^{-3}\,°C^{-1}$ and the sheet resistivity is 13.6 ohm. Fig. 9 shows the experimental *I–V* curves of suspended microstructures. The sheet resistivity is found to be 35 ohm, A negative temperature coefficient of polysilicon resistivity, $-0.35\times10^{-3}\,°C^{-1}$, has been found for these suspended microstructures.

5.2. Power consumption

Previously, we have found that micro thermal bubbles may be generated when the local temperature on microstructures is near the critical temperature of the working liquid [9]. This phenomenon is used in the current experiment for characterizing the electrothermal effects. Fig. 10 shows the power consumption for generating microbubbles in FC 43 (an electronic cooling liquid provided by 3M Company) versus the length of the different microstructures. Solid lines in Fig. 10 are simulation results of power consumption for different widths (1, 2, 5, 10 μm) of attached-type microstructures. Hollow symbols and solid symbols in Fig. 10 are the measured power required to generate thermal bubbles for attached and suspended microstructures, respectively. It is observed in Fig. 10 that suspended microstructures consume less power than attached-type microstructures for reaching bubble-formation temperature. This implies that suspended microstructures have better thermal isolation effects.

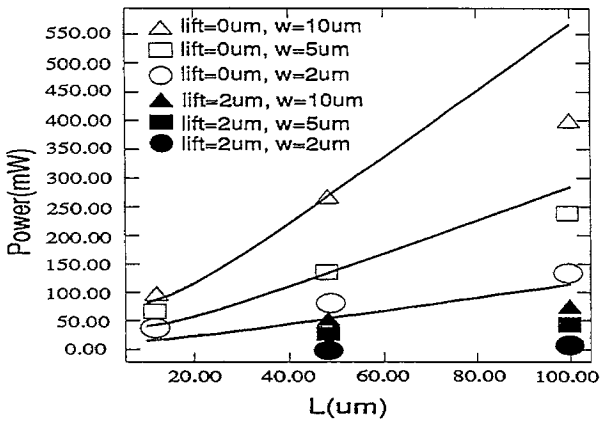

Fig. 10. Comparison of simulation and experimental results of both suspended and attached microstructures.

6. Discussion

Fig. 11 shows two groups of shape factors simulated with fixed *lift*/*h* values but with different *h* values. The solid lines are two suspended microstructures with fixed *lift*/*h* = 1 ratio and the dotted lines are two attached microstructures and *lift*/*h* = 0. The cross represents data for *h* = 1 μm and the open triangle represents data for *h* = 2 μm. For suspended microstructures (solid lines), the shape factors are very close in both cases and a maximum deviation of about 8% occurs at *h*/*w* = 2. However, for attached microstructures, the shape factors have large deviation and the differences reach 54% when *h*/*w* = 2. In both cases, the shape factor increases as the value of *h* increases. The deviation shown in Fig. 11 comes from the fact that the dimensions of the passivation layers remain unchanged even though the dimensions of microstructures and lift distances are proportionally magnified.

In addition to structural dimensions, the thermal property of the working liquid also affects the shape factors. For example, air has a heat conductivity of 0.02624 W $°C^{-1}$ m^{-1}, which is different from that of FC 43 (0.066 W $°C^{-1}$ m^{-1}. Table 1 lists shape factors calculated and used in this paper for both attached and suspended microstructures immersed in air or FC 43. As observed in Table 1, the shape factors for attached-type microstructures are smaller than those of suspended ones. Moreover, for the case of FC 43, higher shape factors are calculated than those in the air environment. Although the above observations are expected by examining the definition of the shape factor, there is no general expression to determine the shape factors of different geometries in different environments.

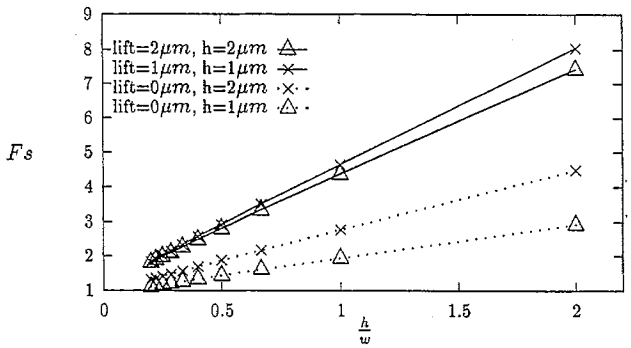

Fig. 11. Variation of shape factors with fixed passivation layers immersed in water. Solid lines are suspended microstructures with *lift*/*h* = 1. Dotted lines are attached microstructures. The cross represents shape factors of *h* = 1 μm and the open triangle represents shape factors of *h* = 2 μm.

Table 1
Shape factors of different types of microstructures in air and FC 43

Width	Suspended type		Attached type	
	Air	FC 43	Air	FC 43
2 μm	3.70	3.73	1.57	1.59
5 μm	2.14	2.15	1.17	1.18
10 μm	1.59	1.60	1.02	1.02

Table 2
Physical properties of microstructures used in the paper

Properties	k_p	k_o	k_n	k_s	C_p	ρ_p
Unit	W (°C m)$^{-1}$	W (°C m)$^{-1}$	W (°C m)$^{-1}$	W (°C m)$^{-1}$	J (kg °C)$^{-1}$	kg m^{-3}
Value	34.0	1.4	3.2	141.0	0.7×10^{3}	2.32×10^{3}

It is noted that our model is fairly correct when the operation temperature is low such that both heat convection and radiation terms are neglected and material properties are assumed to be unchanged. However, these assumptions may not be true under high-temperature operation. From the experimental results and our analytical model, we do not find significant differences of polysilicon physical properties in both polysilicon layers. Table 2 lists all the common properties used in our calculations. These properties were adopted from old IC process data. Newly reported thermal physical properties from the study of a CMOS foundry have similar results [11].

Heat transfer through contact pads has not been considered in our model but it may not be neglected for short microstructures [6]. This effect may cause temperature rises at the contact pad and has been calculated by assuming all the heat flowing into the contact pads goes down to the substrate. The contact pad temperature is estimated as

$$T_{pad}=\frac{\beta T_\infty + k_p A\sqrt{\epsilon}T_r \tanh(\sqrt{\epsilon}L/2)}{\beta + k_p A\sqrt{\epsilon}\tanh(\sqrt{\epsilon}L/2)} \quad (22)$$

where

$$\beta=\frac{k_{att}\times \text{Pad area}}{t_n+t_o} \quad (23)$$

It has been estimated to rise only 1 °C if the whole pad area is assumed to be at one temperature. However, for short structures or regions near contact pads, detailed heat-transfer analysis needs to be further investigated.

7. Conclusions

A one-dimensional process-independent electrothermal model of lineshape microstructures has been established. This model includes a one-dimensional electrothermal analysis and a non-dimensional heat-conduction shape factor, which accounts for heat conduction in dimensions perpendicular to the device axial direction. The shape factors have been simulated and found to increase linearly with respect to the device thickness over width ratio, h/w. Although shape factors can be found by numerical simulation case by case, no general expression can be derived for shape factors in different structural geometries and different environments. Experimental results including I–V curves and bubble-generation tests are consistent with the analytical model. A positive temperature coefficient 2.00×10^{-3} °C^{-1} of polysilicon resistivity has been found for the attached microstructures and a negative temperature coefficient, -0.35×10^{-3} °C^{-1}, has been found for the suspended microstructures. This electrothermal model is useful for lineshape microstructures in electrical or thermal applications.

8. Nomenclature

c_p	specific heat of polysilicon, J (kg °C)$^{-1}$
$F_{s,att}$	excessive thermal conductive shape factor of attached microstructures.
$F_{s,sus}$	excessive thermal conductive shape factor of suspended microstructures.
h	thickness of a lineshape microstructure, m
I	electrical current, A
J	electrical current density, A m^{-2}
k_{att}	combined thermal conductivity of attached microstructures, W (°C m)$^{-1}$
k_{fd}	thermal conductivity of working fluid, W (°C m)$^{-1}$
k_{sus}	combined thermal conductivity of suspended microstructures, W (°C m)$^{-1}$
k_n	thermal conductivity of silicon nitride, W (°C m)$^{-1}$
k_o	thermal conductivity of silicon dioxide, W (°C m)$^{-1}$
k_p	thermal conductivity of polysilicon, W (°C m)$^{-1}$
k_s	thermal conductivity of silicon, W (°C m)$^{-1}$
L	length of a lineshape microstructure, m
R	resistance of a lineshape microstructure, ohm
T	temperature along a lineshape microstructure, °C
$T_{ss,max}$	steady state maximum temperature on a lineshape microstructure, °C
$T(x)_{ss}$	steady state temperature along a lineshape microstructure, °C
$T(x,t)$	transient temperature distribution, °C
T_{avg}	average temperature of a lineshape microstructure, °C
T_r	a reference temperature in heat equation, °C
T_∞	ambient (bulk) temperature, °C
t	time, s
$lift$	suspension distance, m
t_n	thickness of silicon nitride, m
t_o	thickness of silicon dioxide, m
w	width of a lineshape microstructure, m

x	coordinate along the length of a lineshape microstructure
α_p	thermal diffusivity of polysilicon, $m^2\ s^{-1}$
ϵ	a combined variable term in heat equation
ρ_0	resistivity of polysilicon at room temperature, ohm m
ρ_p	density of polysilicon, kg m^{-3}
ξ_p	polysilicon temperature resistivity coefficient, $°C^{-1}$

Acknowledgements

The authors would like to thank the staff at the UC Berkeley Microfabrication Laboratory where the devices were fabricated and 3M Company for providing the test liquid, FC 43. This work was supported by Material R&D Center, Chung-Shan Institute of Science and Technology, Taiwan.

References

[1] R.R Allen, J.D. Meyer and W.R. Knight, Thermodynamics and hydrodynamics of thermal ink jets, *HP Journal, 36* (1985) 21–27.

[2] W. Riethmuller and W. Benecke, Thermally excited silicon microactuators, *IEEE Trans. Electron Devices, ED-35* (1988) 758–762.

[3] D. Moser, R. Lenggenhager and H. Baltes, Silicon gas flow sensors using industrial CMOS and bipolar IC technology, *Sensors and Actuators A, 25–27* (1991) 577–581.

[4] Y.C. Tai and R.S. Muller, Lightly-doped polysilicon bridges as a flow meter, *Sensors and Actuators, 15* (1988) 63–75.

[5] L. Lin, A.P. Pisano and A.P. Lee, Microbubble powered actuator, *Tech. Digest, 6th Int. Conf. Solid-State Sensors and Actuators (Transducers '91), San Francisco, CA, USA, 24–28 June, 1991*, pp. 1041–1044.

[6] G.K. Fedder and R.T. Howe, Thermal assembly of polysilicon microstructures, *IEEE Micro Electro Mechanical Systems (MEMS) Workshop, Nara, Japan, 1991*, pp. 63–68.

[7] C.H. Mastrangelo, J.H. Yeh and R.S. Muller, Electrical and optical characteristics of vacuum-sealed polysilicon microlamps, *IEEE Trans. Electron Devices, ED-39* (1992) 1363–1375.

[8] W.C. Tang, T.H. Nguyen, M.W. Judy and R.T. Howe, Electrostatic-comb drive of lateral polysilicon resonators, *Sensors and Actuators, A21–A23* (1990) 328–331.

[9] L. Lin and A.P. Pisano, Bubble forming on a micro line heater, *American Society of Mechanical Engineers, Dynamic Systems and Control Division DSC, 32* (1991) 147–163.

[10] Swanson Analysis Systems, Inc., *ANSYS Finite Element Analysis Program*, Johnson Road, PO Box 65, Houston, TX 15342-0065, USA.

[11] O. Paul, M. von Arx and H. Baltes, Process-dependent thermophysical properties of CMOS IC thin films, *Tech. Digest, 8th Int. Conf. Solid-State Sensors and Actuators (Transducers '95)/Eurosensors IX, Stockholm, Sweden, 25–29 June, 1995*, Vol. 1, pp. 178–181.

Biographies

Liwei Lin received the B.S. degree in power mechanical engineering from National Tsing Hua University, Taiwan, in 1986 and the M.S. and Ph.D. degrees in mechanical engineering from the University of California, Berkeley, in 1991 and 1993, respectively. He joined BEI Electronics, Inc. from 1993 to 1994 to develop microsensors. Since 1994 he has been an associate professor in the Institute of Applied Mechanics, National Taiwan University. Before going to the USA for graduate study, he served as an instructor in the mechanical engineering department, Chinese Military Academy, Taiwan, from 1986 to 1988. He joined the Berkeley Sensor & Actuator Center, an NSF/Industry/University research cooperative, as a research assistant during his graduate study.His research interests are in microelectromechanical systems, including design modelling and fabrication of microstructures, microsensors and microactuators.

Mu Chiao received his B.S. degree in agricultural mechanical engineering from National Taiwan University, Taiwan, in 1994. He is currently a graduate student in the Institute of Applied Mechanics, National Taiwan University. His research interests are in microelectromechanical systems, including design, modelling and fabrication of microstructures.